

Article

Effects of Waste-Derived ZnO Nanoparticles against Growth of Plant Pathogenic Bacteria and Epidermoid Carcinoma Cells

Titiradsadakorn Jaithon¹, Jittiporn Ruangtong¹, Jiraroj T-Thienprasert^{2,3}
and Nattanan Panjaworayan T-Thienprasert^{1,*} 

¹ Department of Biochemistry, Faculty of Science, Kasetsart University, Bangkok 10900, Thailand; titiradsadakorn.j@ku.th (T.J.); jittiporn.rt@gmail.com (J.R.)

² Department of Physics, Faculty of Science, Kasetsart University, Bangkok 10900, Thailand; chorawut.t@ku.th

³ Thailand Center of Excellence in Physics, Ministry of Higher Education, Science, Research and Innovation, Bangkok 10400, Thailand

* Correspondence: fscinnp@ku.ac.th; Tel.: +66-86-789-9433

Abstract: Green synthesis of zinc oxide nanoparticles (ZnO NPs) has recently gained considerable interest because it is simple, environmentally friendly, and cost-effective. This study therefore aimed to synthesize ZnO NPs by utilizing bioactive compounds derived from waste materials, mangosteen peels, and water hyacinth crude extracts and investigated their antibacterial and anticancer activities. As a result, X-ray diffraction analysis confirmed the presence of ZnO NPs without impurities. An ultraviolet–visible absorption spectrum showed a specific absorbance peak around 365 nm with an average electronic band gap of 2.79 eV and 2.88 eV for ZnO NPs from mangosteen peels and a water hyacinth extract, respectively. An SEM analysis displayed both spherical shapes of ZnO NPs from the mangosteen peel extract (dimension of 154.41 × 172.89 nm) and the water hyacinth extract (dimension of 142.16 × 160.30 nm). Fourier transform infrared spectroscopy further validated the occurrence of bioactive molecules on the produced ZnO NPs. By performing an antibacterial activity assay, these green synthesized ZnO NPs significantly inhibited the growth of *Xanthomonas oryzae* pv. *oryzae*, *Xanthomonas axonopodis* pv. *citri*, and *Ralstonia solanacearum*. Moreover, they demonstrated potent anti-skin cancer activity in vitro. Consequently, this study demonstrated the possibility of using green-synthesized ZnO NPs in the development of antibacterial or anticancer agents. Furthermore, this research raised the prospect of increasing the value of agricultural waste.

Keywords: green synthesis; ZnO nanoparticles; antibacterial activity; anticancer activity; fruit peels; water hyacinth



Citation: Jaithon, T.; Ruangtong, J.; T-Thienprasert, J.; T-Thienprasert, N.P. Effects of Waste-Derived ZnO Nanoparticles against Growth of Plant Pathogenic Bacteria and Epidermoid Carcinoma Cells. *Crystals* **2022**, *12*, 779. <https://doi.org/10.3390/cryst12060779>

Academic Editors: Yamin Leprince-Wang, Guangyin Jing and Basma El Zein

Received: 27 April 2022

Accepted: 24 May 2022

Published: 27 May 2022

Publisher's Note: MDPI stays neutral with regard to jurisdictional claims in published maps and institutional affiliations.



Copyright: © 2022 by the authors. Licensee MDPI, Basel, Switzerland. This article is an open access article distributed under the terms and conditions of the Creative Commons Attribution (CC BY) license (<https://creativecommons.org/licenses/by/4.0/>).

1. Introduction

Zinc oxide nanoparticles (ZnO NPs) are widely used metal oxides due to their dominant properties including photocatalytic properties [1], antimicrobial activity [2–4], anti-inflammatory response [5], anti-cancer activity [6], thermal stability [7], and biocompatibility [8]. Hence, ZnO NPs are applied in a variety of industries, such as agriculture, food processing, cosmetics, medicine, and textiles [9–11].

Chemical and physical approaches are the most common ways to synthesize ZnO NPs [12]. The term “green synthesis” has recently gained popularity due to its simplicity, environmental friendliness, and economic effectiveness. Green synthesis utilizes phytochemicals present in plants, microbes, and fruit peel waste for the bioreduction of metal ions to their corresponding nanoparticles [13,14], which have a variety of particle sizes and shapes [15]. Previous research has shown that using higher concentrations of banana peel extracts resulted in a higher purity of green-produced ZnO NPs with less zinc hydroxide production [16], implying that the phytochemicals present in the extracts act as metal capping agents and/or reducing agents [17]. Subsequently, plant extracts have been proposed to play a role in three different phases of synthesis: (i) reducing agents for the bioreduction

of metal ions or metal salts; (ii) the nanoparticle growth phase; and (iii) stabilizing agents for nanoparticles' final shapes [18,19]. Examples of fruit or vegetable peel extracts that have previously been reported to synthesize ZnO NPs are banana peels [16], citrus peels (orange, lemon, and grape) [20], drumstick peels [21], and onion peels [22].

Mangosteen (*Garcinia mangostana* L.) peels contain abundant amounts of many phytochemicals such as xanthenes, flavonoids, tannins, and anthocyanins [23] and have been demonstrated in vitro to possess antioxidant, anti-inflammatory, antiallergy, antibacterial, and anticancer activities [24,25]. Notably, phytochemicals such as phenolic compounds, terpenoids, alkaloids, vitamins, amino acids, proteins, and glycosides have been used as reducing, capping, and stabilizing agents in nanoparticle formation in a green synthesis method [26–28]. Furthermore, bioactive compounds such as alkaloids, terpenoids, steroids, glycosides, phenols, and flavonoids have also been discovered in water hyacinth (*Eichhornia crassipes*) [29], which is the world's worst invasive aquatic weed [30].

The goal of this study was to utilize a green synthesis approach to synthesize ZnO NPs from crude extracts of mangosteen peels and water hyacinth. Subsequently, antibacterial activity against plant pathogen diseases including *Xanthomonas oryzae* pv. *oryzae* (rice bacterial blight pathogen), *Xanthomonas axonopodis* pv. *citri* (citrus canker disease), and *Ralstonia solanacearum* (bacterial wilt disease) and anticancer activity against epidermoid cancer cells (A431) of newly synthesized ZnO NPs were investigated.

2. Materials and Methods

2.1. Preparation of Crude Extracts

In May, mangosteen peels were collected from households in Phayao District, Phayao province, Northern Thailand. Freshwater hyacinth was collected from the canal in Bann Na District, Nakhon Nayok, Thailand. All samples were shed dried and ground into powder. Next, 2 g of ground mangosteen peels were extracted in 500 mL of deionized water at room temperature for 30 min. Then, a crude extract was prepared as described in [6]. For water hyacinth extraction, the preparation was performed as described in [31]. After filtration, the crude extracts were refrigerated at 4 °C until next use.

2.2. Green Synthesis of ZnO NPs

For the synthesis of ZnO NPs from mangosteen peels, 50 mL of 2 M zinc acetate solution ($\text{Zn}(\text{CH}_3\text{COO})_2$, LOBA chemie, Maharashtra, India) was prepared in deionized water for 20 min at room temperature with continual stirring. After that, each burette was filled with 100 mL of the crude extract and 100 mL of the precursor, which were then dropped into a beaker dropwise. The mixed solution was kept stirring for 1 h at room temperature. The mixture was then mixed dropwise with 2 M of NaOH (KEMAUS, Sydney, Australia) until it reached pH 12 and further agitated for 1 h. The mixture was further centrifuged for 30 min at $8000 \times g$ at 4 °C. The precipitates were filtered and dried overnight at 80 °C. For the green synthesis of ZnO NPs using water hyacinth, the procedure was performed as described in [31].

2.3. X-ray Diffraction (XRD) Analysis

The diffraction pattern was analyzed using an X-ray diffractometer (Bruker D8 Advance, MA, USA) with $\text{CuK}\alpha$ radiation and wavelength (λ) = 1.541 Å. The diffraction intensity was measured in the 2θ ranging between 20° and 80°. After that, the phases of the ZnO wurtzite were compared using JCPDS number 00036-1451 [32]. Then, Rietveld refinement was used to determine the lattice parameters and crystalline sizes using MAUD software (Trento, Italy) [33–35].

2.4. Ultraviolet-Visible (UV-Vis) Spectroscopy

In the photoluminescence mode of a UV-1800 spectrophotometer (SHIMADZU, Kyoto, Japan), the dispersed ZnO NPs in deionized water were investigated for absorption spectra between 300 and 600 nm. The optical band gap of the generated ZnO NPs was then calculated using the Tauc plot [36].

2.5. Scanning Electron Microscopy (SEM)

The ZnO NPs were prepared using a Mini Sputter Coater (SC7620, Quorum Technologies Ltd., Kent, UK), and their morphology was analyzed using FEI Quanta 450 (OR, USA) as described in [6]. ImageJ program [37] was also used to determine the particle sizes.

2.6. Fourier Transform Infrared (FT-IR) Analysis

To investigate the functional group of the synthesized ZnO NPs, FT-IR analysis was performed using an FT-IR spectrometer (Bruker, MA, USA). The samples were operated using a potassium bromide (KBr) approach with an infrared region of 400 to 4000 cm^{-1} and a 4 cm^{-1} resolution. The covalent bonds between the zinc metal and oxygen atoms (Zn-O) were observed in a range between 400 to 600 cm^{-1} .

2.7. Antibacterial Activity Test

The antibacterial activity of the ZnO NPs was tested against *Xanthomonas oryzae* pv. *oryzae* (rice bacterial blight pathogen), *Xanthomonas axonopodis* pv. *citri* (citrus canker disease), and *Ralstonia solanacearum* (bacterial wilt disease). These bacterial strains were isolated, characterized, and identified by the Plant Protection Research and Development Office, Bangkok, Thailand. Bacteria cultures were prepared by inoculating the strains in Luria broth (LB) with shaking at 37 °C until the OD₆₀₀ reached 0.6. Then, 500 μL of the cultures were treated with various concentrations of ZnO NPs ranging from 0–10 mg/mL and further incubated with shaking at 37 °C for 24 h. Next, the UV-Vis spectroscopic analysis was performed at 600 nm (SHIMADZU, Kyoto, Japan). The experiment was performed in two independent experiments with quadruplicate. The percentage of cell growth was determined as follows: $\text{Bacteria Growth (\%)} = [(A_{\text{ZnO NPs}} - A_{\text{Blank}}) / (A_{\text{Control}} - A_{\text{Blank}})] \times 100$, where $A_{\text{ZnO NPs}}$ is the mean absorbance value for the culture treated with ZnO NPs, A_{Blank} is the mean absorbance value for the ZnO NPs solution, and A_{Control} is the mean absorbance for the culture only (without ZnO NPs treatment). Then, the half-maximal inhibitory concentration (IC₅₀) values of the ZnO NPs against the bacterial growth were calculated using GraphPad QuickCalcs (GraphPad software Prism 9, CA, USA).

2.8. Cell Viability Assay, MTT Assay

Skin cancer cells (A431; ATCC[®] CRL1555[™]) and an immortalized human keratinocyte cell line (HaCaT; CLS 300493) were seeded approximately 1.5×10^4 cells per well into 96 well-plates (Falcon[®] a Corning brand, USA) at 37 °C. After 24 h of incubation, the cells were treated with dispersed ZnO NPs in deionized water in different concentrations ranging from 7.8–1000 $\mu\text{g/mL}$ and further incubated at 37 °C for 96 h. The cells were then incubated for 3 h with an MTT solution. To dissolve the formazan, 50 μL of dimethyl sulfoxide (Fisher Scientific, Hampton, NH, USA) was added. Next, the absorbance was measured at 570 nm using a microplate reader (Sunrise-Basic TECAN, Männedorf, Switzerland). The cell viability (%) was calculated as described in [38].

2.9. Statistical Analysis

The significant differences between the samples were compared by ANOVA Tukey's multiple comparison (GraphPad Software Prism9, San Diego, CA, USA).

3. Results

3.1. Green Synthesis of ZnO NPs Using Mangosteen Peels and Water Hyacinth Crude Extracts

The green synthesis was carried out in four steps: the preparation of a water crude extract, the preparation of a precursor solution, a green synthesis reaction, and particle collection, as shown in Figure 1.

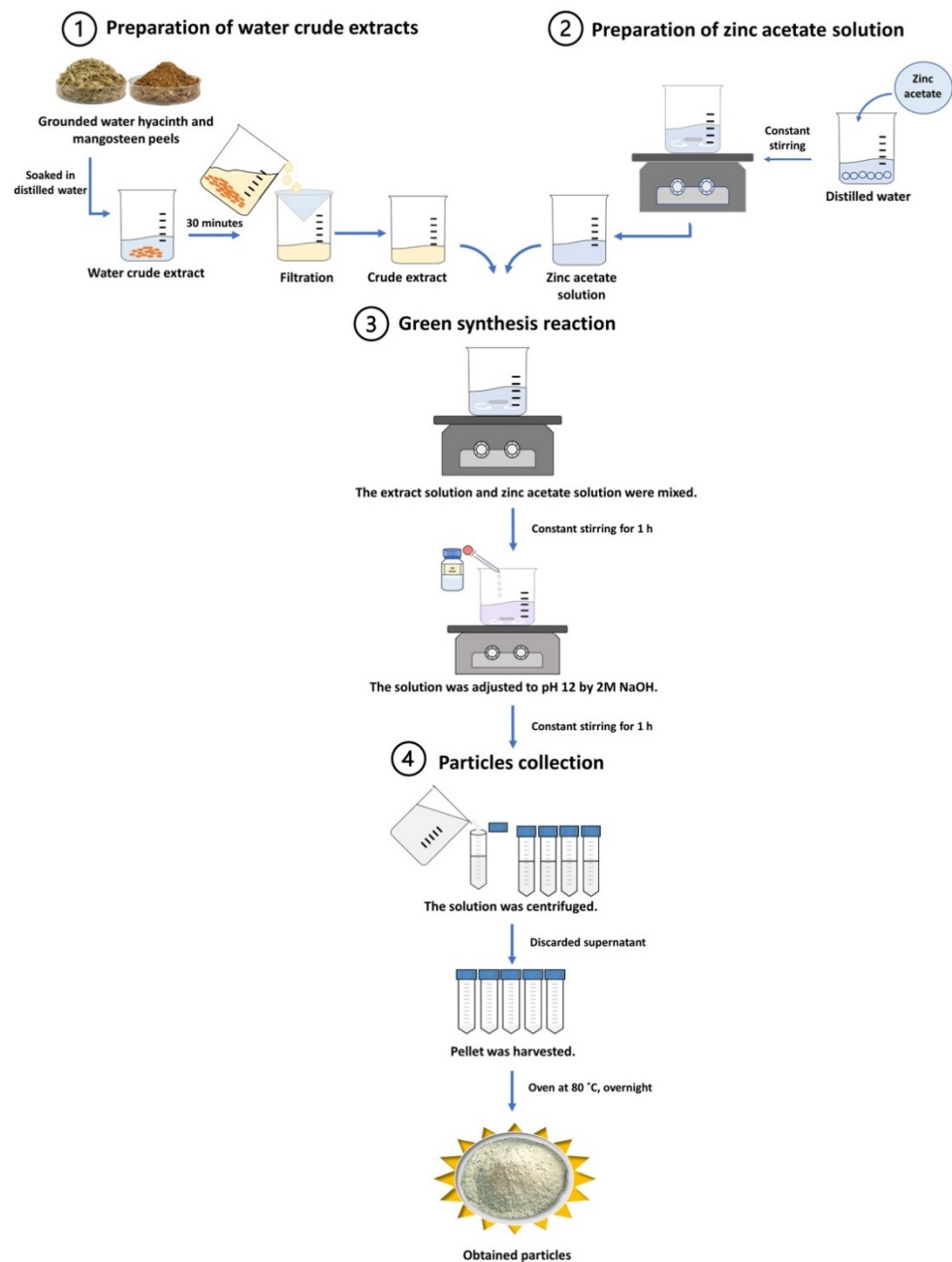


Figure 1. Schematic illustration of green synthesis using mangosteen peels and water hyacinth.

For the synthesis of ZnO NPs using mangosteen peel extract, the color of crude extract appeared in pale yellow. The reaction mixture of zinc acetate and the crude extract was purple-blueish in appearance. After pH adjustment, the precipitant was observed to be white in color, implying the formation of ZnO NPs. Likewise, the zinc acetate and crude extract reaction mixture was white in color after pH correction, despite the pale green color of the water hyacinth crude extract. The precipitant was also white, suggesting the presence of ZnO NPs (data not shown).

Notably, the particles obtained from the synthesis of the mangosteen (*Garcinia mangostana* L.) peel extract were designated as ZnO-Gm, whereas ZnO-Ec was obtained from the green synthesis of the water hyacinth (*Eichhornia crassipes*) extract.

3.1.1. The ZnO Wurtzite Structure Has Been Identified in All Synthesis Samples

Using XRD analysis, the XRD pattern confirmed that the synthesis process successfully synthesized the ZnO wurtzite structure from both the mangosteen peels and water hyacinth crude extracts without the impurity of other particles. The higher peak intensity obtained from ZnO-Ec indicates the better crystallinity of ZnO NPs (Figure 2).

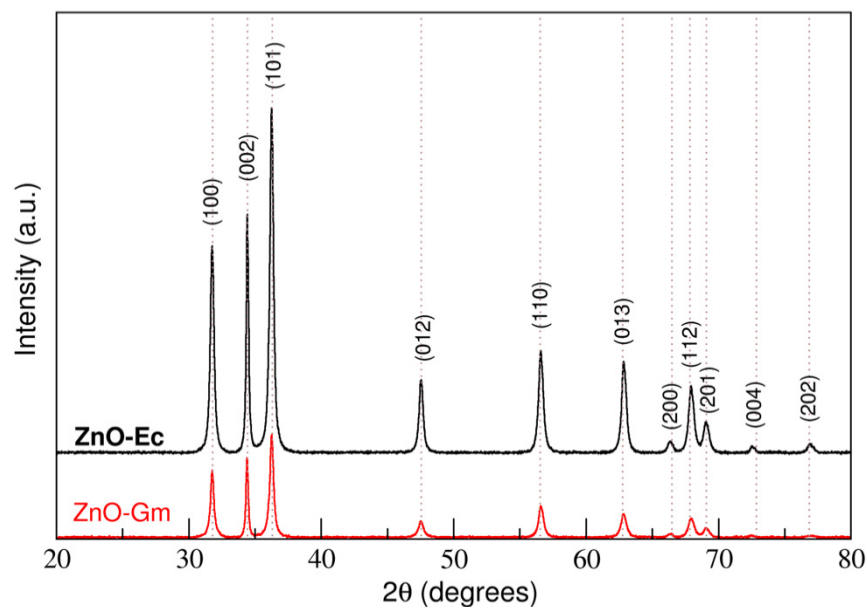


Figure 2. XRD analysis of synthesized ZnO particles prepared by mangosteen (*G. mangostana*) peel extract, ZnO-Gm; and whole water hyacinth (*E. crassipes*), ZnO-Ec.

Next, Rietveld refinement was used to calculate the lattice parameters and crystalline sizes of the synthesized ZnO NPs using MAUD software. ZnO-Gm and ZnO-Ec had lattice parameters of $a = 3.2536 \text{ \AA}$, $c = 5.2155 \text{ \AA}$, and $a = 3.2545 \text{ \AA}$, $c = 5.2126 \text{ \AA}$, respectively. ZnO-Gm (290.42 \AA) showed slightly smaller estimated crystalline sizes than ZnO-Ec (318.99 \AA). (Table 1).

Table 1. The lattice parameters and crystalline sizes for synthesized ZnO NPs determined from XRD data after Rietveld refinement.

ZnO NPs	a (\AA)	c (\AA)	Crystalline Size (\AA)
ZnO-Gm	3.2536	5.2155	290.42
ZnO-Ec	3.2545	5.2126	318.99

3.1.2. UV–Visible Absorption Spectra and Optical Band Gap of Newly Synthesized ZnO Particles

Both ZnO-Gm and ZnO-Ec revealed absorption spectra in the UV region at 365 nm. The ZnO-Gm and ZnO-Ec samples have average energy band gaps of 2.79 eV and 2.88 eV, respectively (Figure 3).

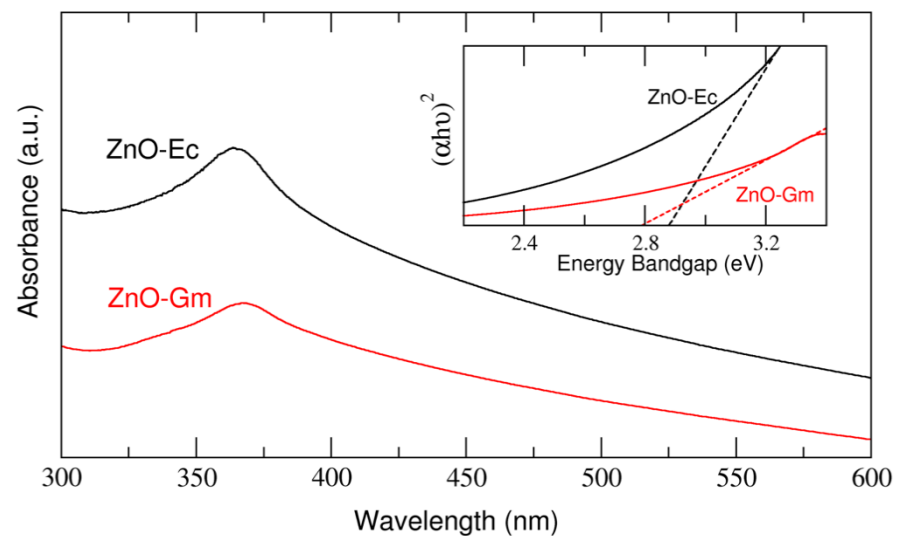


Figure 3. UV-Vis spectra and energy band gap of green synthesized ZnO samples. ZnO-Gm nanoparticles produced from mangosteen peel crude extract whereas ZnO-Ec samples generated from water hyacinth crude extract.

3.1.3. Morphology and Size of Newly Synthesized ZnO NPs

To determine the morphology and sizes of ZnO-Gm and ZnO-Ec, SEM analysis was performed. Despite the use of different types of crude extracts in the synthesis, SEM images demonstrated round, almost spherical shapes of the synthesized ZnO particles, (Figure 4). The ZnO-Gm particles were 154.41×172.89 nm in size, while the ZnO-Ec particles were slightly smaller, averaging 142.16×160.30 nm (Figure 4).

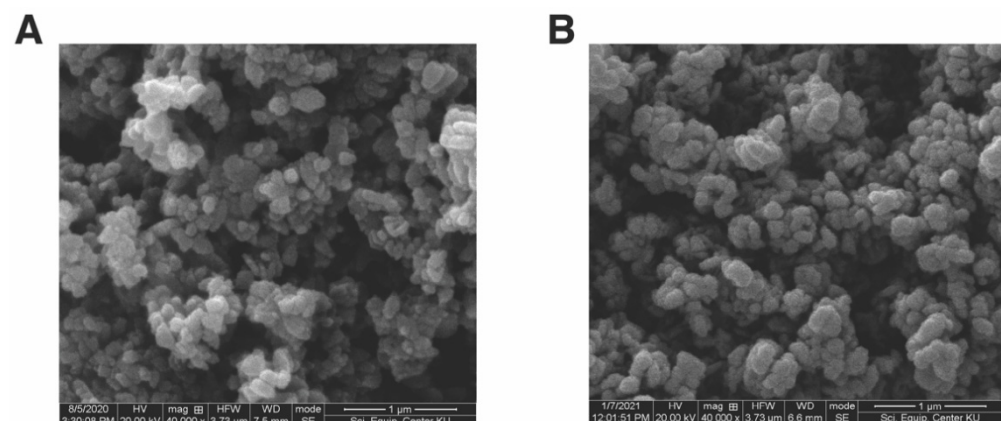


Figure 4. SEM images of synthesized ZnO NPs. (A) ZnO-Gm (mangosteen peel extract) and (B) ZnO-Ec (water hyacinth).

3.1.4. FTIR Analysis of Synthesized ZnO NPs

Next, FTIR was then used to identify the functional groups involved in the formation of the ZnO NPs. As a result, the spectral peaks between 700 and 500 cm^{-1} indicated the formation of ZnO NPs in both ZnO-Gm and ZnO-Ec. Furthermore, the broad peak at around 3500 cm^{-1} implied the stretching vibration of O—H stretching. Both ZnO-Gm and ZnO-Ec also presented peaks in the region around 1500 cm^{-1} , suggesting carbonyl stretching (C—O) (Figure 5).

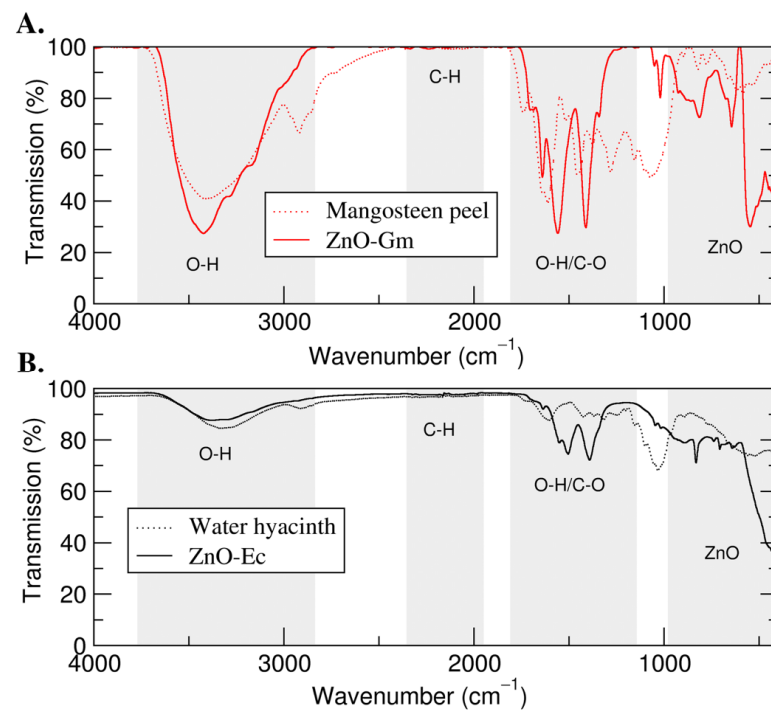


Figure 5. FTIR analysis of green synthesized ZnO NPs. (A) ZnO-Gm generated from mangosteen peel extract; (B) ZnO-Ec produced from water hyacinth extract.

3.2. Synthesized ZnO NPs Drastically Inhibited Growth of Plant Pathogenic Bacteria

From Figure 6, the results showed that both ZnO-Gm and ZnO-Ec particles significantly inhibited all the tested plant pathogenic bacteria. Furthermore, ZnO-Gm demonstrated almost 2-fold greater antibacterial activity than ZnO-Ec, with IC_{50} values of 1.887 mg/mL, 1.802 mg/mL, and 1.800 mg/mL, against *X. oryzae* pv. *oryzae*, *R. solanacearum*, and *X. axonopodis* pv. *citri*, respectively (Figure 6D). In addition, the IC_{50} values of ZnO-Gm for *X. oryzae* pv. *oryzae*, *R. solanacearum*, and *X. axonopodis* pv. *citri* were 3.970 mg/mL, 3.835 mg/mL, and 3.385 mg/mL, respectively (Figure 6D). The inhibitory effects were caused by the synthesized ZnO NPs, not the mangosteen peel extract or water hyacinth extract, because the extract at the same concentration as the ZnO NPs showed no antibacterial activity (data not shown).

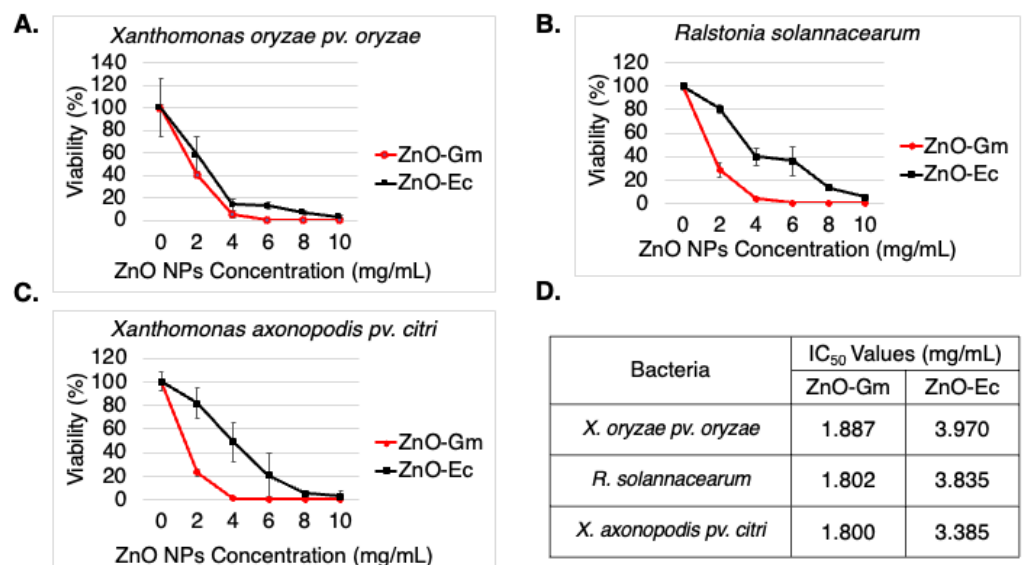


Figure 6. Synthesized ZnO NPs possessed antibacterial activity (A) Viability (%) of *Xanthomonas oryzae* pv. *oryzae* (rice bacterial blight pathogen), (B) Viability (%) of *Xanthomonas axonopodis* pv. *citri*

(citrus canker disease), (C) Viability (%) of *Ralstonia solanacearum* (bacterial wilt disease), (D) IC₅₀ values of ZnO-Gm and ZnO-Gc against tested bacteria in the study. The data are represented in quadruplicate of mean ± SD from at least three independent experiments.

3.3. Synthesized ZnO NPs Possessed Anticancer Activity against Skin Cancer Cells

To investigate anti-skin cancer activity, a non-melanoma skin cancer cell (A431) [39] and an intermediate cancerous skin carcinoma cell, HaCaT [40], were treated with different concentrations of either ZnO-Gm and ZnO-Ec ranging from 0–1000 µg/mL. The experiments also included a normal cell, Vero, and the effects of crude extracts, mangosteen peel and water hyacinth. As a result, both ZnO-Gm and ZnO-Ec dramatically reduced cell viability in a dose-dependent manner, with greater inhibitory effects against A431 and HaCaT cells than Vero cells (Figures 7 and 8). In contrast, the mangosteen peel extract and water hyacinth extract showed no inhibitory effects on any cells at the concentrations tested (Figures 7 and 8). The IC₅₀ values of ZnO-Gm were 28 µg/mL, 39 µg/mL, and 145.6 µg/mL for HaCaT, A431, and Vero cells, respectively (Figure 7).

On the other hand, the IC₅₀ values of ZnO-Ec were 79.5 µg/mL, 10.12 µg/mL, and 162 µg/mL (Figure 8).

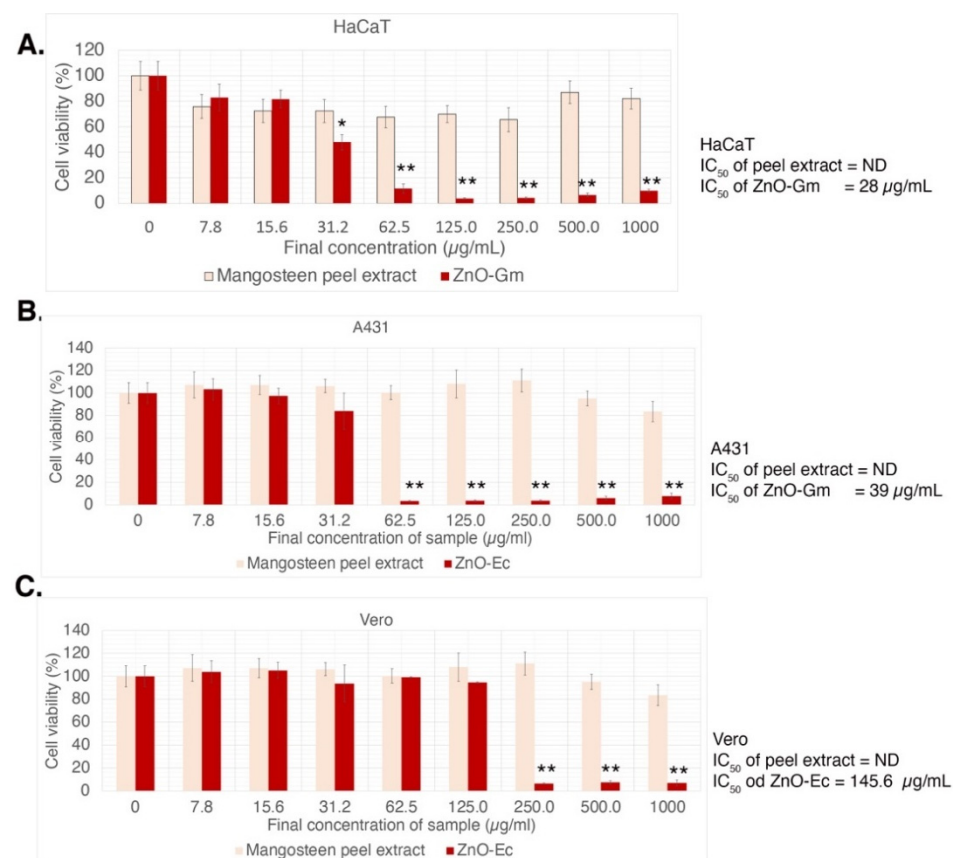


Figure 7. Cytotoxicity effects of ZnO-Gm and mangosteen extract in vitro. (A) HaCaT, (B) A431, and (C) Vero. ND stands for not determined. IC₅₀ values were shown as indicated. The data are represented in quadruplicate of mean ± SD from three independent experiments. The significant differences between the samples were shown as * $p < 0.05$, ** $p < 0.01$ (by ANOVA, Tukey's test).

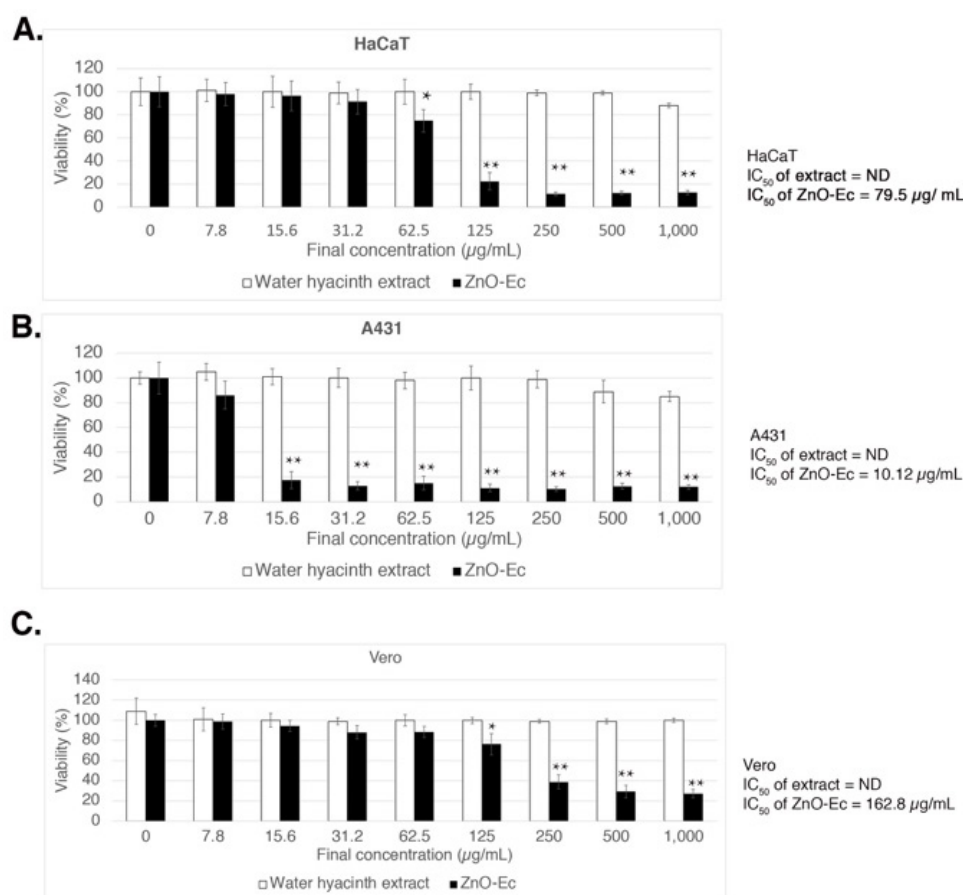


Figure 8. Cytotoxicity effects of ZnO-Ec and water hyacinth crude extract in vitro. (A) HaCaT, (B) A431, and (C) Vero. ND stands for not determined. IC_{50} values were shown as indicated. The results are presented as mean \pm SD of quadruplicate data from three independent experiments. * $p < 0.05$, ** $p < 0.01$ (using ANOVA, Tukey's test) were used to indicate significant differences between the samples.

4. Discussion

Using a green synthesis method, this study newly synthesized ZnO NPs from mangosteen peel and water hyacinth crude extracts, which were designated as ZnO-Gm and ZnO-Ec, respectively. The results implied that mangosteen peel and water hyacinth extracts contained bioactive compounds that served as reducing agents and capping agents that react with zinc acetate solution to form ZnO NPs. Phytochemicals found in mangosteen peels include xanthenes, flavonoids, tannins, and anthocyanins [23], whereas water hyacinth contains alkaloids, terpenoids, steroids, glycosides, phenols, and flavonoids [29]. Both ZnO-Gm and ZnO-Ec displayed absorption maxima about 365 nm, which is consistent with previous results using *Coccinia abyssinica* [41], *Cratoxylum formosum* [6], and *Coriandrum sativum* [42,43], but differs from ZnO bulk, which occurs at around 373 nm [44,45]. Notably, ZnO NPs typically have a band gap of 3.37 eV [46], and thus synthesized ZnO-Gm and ZnO-Ec are narrow-band-gap ZnO NPs with 2.79 eV and 2.88 eV, respectively. This narrow band gap is likely due to the organic molecules of the extracts attached on the surface of ZnO NPs [47]. According to prior research, the plant species, concentration of extract, precursor concentration, duration of synthesis, pH condition, and calcination temperature are six key characteristics that can influence ZnO NPs morphology (see review [48]). Despite using distinct types of plant crude extracts, this study generated green ZnO NPs in spherical shapes with slightly different sizes from mangosteen peel extract and water hyacinth extract.

According to antibacterial activity assays, this study provided additional knowledge indicating that the green synthesized ZnO NPs from mangosteen peel and water hyacinth

extracts effectively inhibited various plant pathogenic bacteria including *Xanthomonas oryzae* pv. *oryzae* (rice bacterial blight pathogen), *Xanthomonas axonopodis* pv. *citri* (citrus canker disease), and *Ralstonia solanacearum* (bacterial wilt disease). In comparison to previous studies, the IC₅₀ of the generated ZnO NPs (1.80–3.97 mg/mL) demonstrated more potent suppression against *X. oryzae* pv. *oryzae* than the IC₅₀ of methanol extracts of *Piper sarmentosum* fruit and leaves (8.41 mg/mL and 24.69 mg/mL, respectively) [49], but the IC₅₀ of the produced ZnO NPs against *X. oryzae* pv. *oryzae* were less strong than IC₅₀ of melittin (about 9–10 µM) [50] and IC₅₀ of resveratrol (11.67 ± 0.58 µg/mL) [51]. The synthesized ZnO NPs, on the other hand, displayed lower IC₅₀ against *X. axonopodis* pv. *citri* and *R. solanacearum* than streptomycin sulfate (6.94 µg/mL and 7.63 µg/mL, respectively) [52]. Our antibacterial activity assay was carried out in the dark inside an incubator, and thus there were no photocatalytic effects, which could lead to poorer bacterial growth suppression. We are currently evaluating the antibacterial properties of synthesized ZnO NPs against plant pathogens on crop fields to prove this hypothesis. Interestingly, despite their similar form and size, ZnO-Gm had more potent antibacterial activity than ZnO-Ec. We hypothesized that it was because ZnO-Gm presents more higher functional groups of phytochemicals on its surface than ZnO-Ec based on the FTIR and energy band gap analyses. Previous research has also proposed that the addition of phytochemicals on the surface of ZnO NPs could improve their anticancer efficacy [6]. Furthermore, Kalachyova et al. (2017) demonstrated that the bonded chemical functional groups were important for the light-induced antibacterial activities of surface-modified gold multibranched nanoparticles [53].

In contrast to chemotherapeutic drugs, ZnO NPs have been found to exhibit low toxicity, biodegradability, and therapeutic effects with a high degree of cancer selectivity [54,55]. This study showed that low doses of ZnO-Gm and ZnO-Ec (<80 µg/mL) significantly reduced cell viability by more than 50% inhibition against epidermoid carcinoma cells (A431) and very early-stage cells in skin tumorigenesis (HaCaT) without causing cytotoxicity in normal cells. Likewise, the green synthesis of ZnO NPs from rhizomes of *Alpinia calcarata* also inhibited the growth of A431 [56]. Furthermore, green ZnO NPs from a *Cratoxylum formosum* leaf extract were previously shown to drastically inhibit A431 by upregulating transcripts involved in the inflammatory response and downregulating transcripts that promote cell proliferation [6]. Even though ZnO NPs have shown significant promise in the treatment of skin cancer, further research and the in-depth understanding of cellular and molecular pathways, as well as clinical studies, will be required in the future for the development of cancer therapies.

5. Conclusions

This study highlighted the green synthesis of ZnO NPs from mangosteen peel extract (ZnO-Gm) and water hyacinth extract (ZnO-Ec). The spherical forms of ZnO-Gm (dimensions of 154.41 × 172.89 nm) and ZnO-Ec (dimensions of 142.16 × 160.30 nm) were obtained without the presence of additional crystalline impurities. The energy band gaps of ZnO-Gm were 2.79 eV, whereas for ZnO-Ec, they were 2.88 eV. Both synthesized ZnO NPs showed a specific absorbance peak around 365 nm, and their surfaces had bioactive functional groups from the extracts. The green-synthesized ZnO NPs significantly inhibited the growth of pathogenic plant bacteria including *Xanthomonas oryzae* pv. *oryzae*, *Xanthomonas axonopodis* pv. *citri*, and *Ralstonia solanacearum*. Moreover, they possessed potent anti-skin-cancer activity in vitro.

Author Contributions: Conceptualization, T.J. and N.P.T.-T.; methodology, N.P.T.-T.; validation, T.J., J.R., J.T.-T. and N.P.T.-T.; formal analysis, T.J., J.T.-T. and N.P.T.-T.; investigation, T.J. and J.R.; data curation, J.T.-T. and N.P.T.-T.; writing—original draft preparation, T.J., J.T.-T. and N.P.T.-T.; writing—review and editing, N.P.T.-T.; visualization, T.J., J.R., J.T.-T. and N.P.T.-T.; supervision, J.T.-T. and N.P.T.-T.; project administration, N.P.T.-T.; funding acquisition, T.J., J.R., J.T.-T. and N.P.T.-T. All authors have read and agreed to the published version of the manuscript.

Funding: This research was funded by Kasetsart University through the Graduate School Fellowship Program. N.P.T.-T. was funded by the National Research Council of Thailand (Aor-Por-Sor 96/2563). J.T.-T. and N.P.T.-T. have been supported by Kasetsart University Research and Development Institute (KURDI), Bangkok, Thailand.

Institutional Review Board Statement: Not applicable for studies not involving humans or animals.

Informed Consent Statement: Not applicable.

Data Availability Statement: Data available on request. The data presented in this study are available on request from the corresponding author.

Acknowledgments: Our most heartfelt thanks to Kamonrat Sukchom for collecting and processing water hyacinth samples, as well as to Wannaporn Kaewduanglek for preliminary data of green-synthesized ZnO NPs using water hyacinth extract.

Conflicts of Interest: The authors declare no conflict of interest.

References

1. Adeel, M.; Saeed, M.; Khan, I.; Muneer, M.; Akram, N. Synthesis and Characterization of Co-ZnO and Evaluation of Its Photocatalytic Activity for Photodegradation of Methyl Orange. *ACS Omega* **2021**, *6*, 1426–1435. [[CrossRef](#)] [[PubMed](#)]
2. Jiang, S.; Lin, K.; Cai, M. ZnO Nanomaterials: Current Advancements in Antibacterial Mechanisms and Applications. *Front. Chem.* **2020**, *8*, 580. [[CrossRef](#)] [[PubMed](#)]
3. Siddiqi, K.S.; ur Rahman, A.; Tajuddin Husen, A. Properties of Zinc Oxide Nanoparticles and Their Activity Against Microbes. *Nanoscale Res. Lett.* **2018**, *13*, 141. [[CrossRef](#)] [[PubMed](#)]
4. Burmistrov, D.E.; Simakin, A.V.; Smirnova, V.V.; Uvarov, O.V.; Ivashkin, P.I.; Kucherov, R.N.; Ivanov, V.E.; Bruskov, V.I.; Sevostyanov, M.A.; Baikina, A.S.; et al. Bacteriostatic and Cytotoxic Properties of Composite Material Based on ZnO Nanoparticles in PLGA Obtained by Low Temperature Method. *Polymers* **2021**, *14*, 49. [[CrossRef](#)]
5. Nagajyothi, P.C.; Cha, S.J.; Yang, I.J.; Sreekanth, T.V.M.; Kim, K.J.; Shin, H.M. Antioxidant and anti-inflammatory activities of zinc oxide nanoparticles synthesized using Polygala tenuifolia root extract. *J. Photochem. Photobiol. B Biol.* **2015**, *146*, 10–17. [[CrossRef](#)]
6. Jevapatarakul, D.; T-Thienprasert, J.; Payungporn, S.; Chavalit, T.; Khamwut, A.; T-Thienprasert, N.P. Utilization of Cratogeomys formosum crude extract for synthesis of ZnO nanosheets: Characterization, biological activities and effects on gene expression of nonmelanoma skin cancer cell. *Biomed. Pharmacother.* **2020**, *130*, 110552. [[CrossRef](#)]
7. Srivastava, N.; Srivastava, M.; Mishra, P.K.; Ramteke, P.W. Application of ZnO Nanoparticles for Improving the Thermal and pH Stability of Crude Cellulase Obtained from *Aspergillus fumigatus* AA001. *Front. Microbiol.* **2016**, *7*, 514. [[CrossRef](#)]
8. Zhou, J.; Xu, N.S.; Wang, Z.L. Dissolving behavior and stability of ZnO wires in biofluids: A study on biodegradability and biocompatibility of ZnO nanostructures. *Adv. Mater.* **2006**, *18*, 2432–2435. [[CrossRef](#)]
9. Verbič, A.; Gorjanc, M.; Simončič, B. Zinc Oxide for Functional Textile Coatings: Recent Advances. *Coatings* **2019**, *9*, 550. [[CrossRef](#)]
10. Sabir, S.; Arshad, M.; Chaudhari, S.K. Zinc Oxide Nanoparticles for Revolutionizing Agriculture: Synthesis and Applications. *Sci. World J.* **2014**, *2014*, 925494. [[CrossRef](#)]
11. Mishra, P.K.; Mishra, H.; Ekielski, A.; Talegaonkar, S.; Vaidya, B. Zinc oxide nanoparticles: A promising nanomaterial for biomedical applications. *Drug Discov. Today* **2017**, *22*, 1825–1834. [[CrossRef](#)] [[PubMed](#)]
12. Singh, T.A.; Sharma, A.; Tejwan, N.; Ghosh, N.; Das, J.; Sil, P.C. A state of the art review on the synthesis, antibacterial, antioxidant, antidiabetic and tissue regeneration activities of zinc oxide nanoparticles. *Adv. Colloid Interface Sci.* **2021**, *295*, 102495. [[CrossRef](#)] [[PubMed](#)]
13. Agarwal, H.; Venkat Kumar, S.; Rajeshkumar, S. A review on green synthesis of zinc oxide nanoparticles—An eco-friendly approach. *Resour.-Effic. Technol.* **2017**, *3*, 406–413. [[CrossRef](#)]
14. Noah, N.M.; Ndangili, P.M. Green synthesis of nanomaterials from sustainable materials for biosensors and drug delivery. *Sens. Int.* **2022**, *3*, 100166. [[CrossRef](#)]
15. Jamdagni, P.; Khatri, P.; Rana, J.S. Green synthesis of zinc oxide nanoparticles using flower extract of *Nyctanthes arbor-tristis* and their antifungal activity. *J. King Saud Univ.-Sci.* **2018**, *30*, 168–175. [[CrossRef](#)]
16. Ruangtong, J.; T-Thienprasert, J.; T-Thienprasert, N.P. Green synthesized ZnO nanosheets from banana peel extract possess anti-bacterial activity and anti-cancer activity. *Mater. Today Commun.* **2020**, *24*, 101224. [[CrossRef](#)]
17. Basnet, P.; Inakhunbi Chanu, T.; Samanta, D.; Chatterjee, S. A review on bio-synthesized zinc oxide nanoparticles using plant extracts as reductants and stabilizing agents. *J. Photochem. Photobiol. B Biol.* **2018**, *183*, 201–221. [[CrossRef](#)]
18. Singh, J.; Dutta, T.; Kim, K.-H.; Rawat, M.; Samddar, P.; Kumar, P. ‘Green’ synthesis of metals and their oxide nanoparticles: Applications for environmental remediation. *J. Nanobiotechnol.* **2018**, *16*, 84. [[CrossRef](#)]
19. Makarov, V.V.; Love, A.J.; Sinitsyna, O.V.; Makarova, S.S.; Yaminsky, I.V.; Taliansky, M.E.; Kalinina, N.O. “Green” nanotechnologies: Synthesis of metal nanoparticles using plants. *Acta Nat.* **2014**, *6*, 35–44. [[CrossRef](#)]
20. Okpara, E.C.; Fayemi, O.E.; Sherif, E.-S.M.; Junaedi, H.; Ebenso, E.E. Green Wastes Mediated Zinc Oxide Nanoparticles: Synthesis, Characterization and Electrochemical Studies. *Materials* **2020**, *13*, 4241. [[CrossRef](#)]

21. Surendra, T.V.; Roopan, S.M.; Al-Dhabi, N.A.; Arasu, M.V.; Sarkar, G.; Suthindhiran, K. Vegetable Peel Waste for the Production of ZnO Nanoparticles and its Toxicological Efficiency, Antifungal, Hemolytic, and Antibacterial Activities. *Nanoscale Res. Lett.* **2016**, *11*, 546. [[CrossRef](#)] [[PubMed](#)]
22. Modi, S.; Yadav, V.K.; Choudhary, N.; Alswieleh, A.M.; Sharma, A.K.; Bhardwaj, A.K.; Khan, S.H.; Yadav, K.K.; Cheon, J.-K.; Jeon, B.-H. Onion Peel Waste Mediated-Green Synthesis of Zinc Oxide Nanoparticles and Their Phytotoxicity on Mung Bean and Wheat Plant Growth. *Materials* **2022**, *15*, 2393. [[CrossRef](#)] [[PubMed](#)]
23. Aizat, W.M.; Jamil, I.N.; Ahmad-Hashim, F.H.; Noor, N.M. Recent updates on metabolite composition and medicinal benefits of mangosteen plant. *PeerJ* **2019**, *7*, e6324. [[CrossRef](#)] [[PubMed](#)]
24. Shan, T.; Ma, Q.; Guo, K.; Liu, J.; Li, W.; Wang, F.; Wu, E. Xanthones from mangosteen extracts as natural chemopreventive agents: Potential anticancer drugs. *Curr. Mol. Med.* **2011**, *11*, 666–677. [[CrossRef](#)] [[PubMed](#)]
25. Suttirak, W.; Manurakchinakorn, S. In vitro antioxidant properties of mangosteen peel extract. *J Food Sci. Technol.* **2014**, *51*, 3546–3558. [[CrossRef](#)]
26. Akhtar, M.S.; Panwar, J.; Yun, Y.-S. Biogenic Synthesis of Metallic Nanoparticles by Plant Extracts. *ACS Sustain. Chem. Eng.* **2013**, *1*, 591–602. [[CrossRef](#)]
27. Ghosh, P.R.; Fawcett, D.; Sharma, S.B.; Poinern, G.E.J. Production of High-Value Nanoparticles via Biogenic Processes Using Aquacultural and Horticultural Food Waste. *Materials* **2017**, *10*, 852. [[CrossRef](#)]
28. Korbekandi, H.; Irvani SFau-Abbasi, S.; Abbasi, S. Production of nanoparticles using organisms. *Crit. Rev. Biotechnol.* **2009**, *29*, 279–306. [[CrossRef](#)]
29. Guna, V.; Ilangovan, M.; Anantha Prasad, M.G.; Reddy, N. Water Hyacinth: A Unique Source for Sustainable Materials and Products. *ACS Sustainable Chem. Eng.* **2017**, *5*, 4478–4490. [[CrossRef](#)]
30. Kathiresan, R.M. Allelopathic potential of native plants against water hyacinth. *Crop Prot.* **2000**, *19*, 705–708. [[CrossRef](#)]
31. T-Thienprasert, N.P.; T-Thienprasert, J.; Ruangtong, J.; Jaithon, T.; Srifah Huehne, P.; Piasai, O. Large Scale Synthesis of Green Synthesized Zinc Oxide Nanoparticles from Banana Peel Extracts and Their Inhibitory Effects against *Colletotrichum* sp., Isolate KUFC 021, Causal Agent of Anthracnose on *Dendrobium* Orchid. *J. Nanomater.* **2021**, *2021*, 5625199. [[CrossRef](#)]
32. Jenkins, R.; Fawcett, T.G.; Smith, D.K.; Visser, J.W.; Morris, M.C.; Frevel, L.K. JCPDS—International Centre for Diffraction Data Sample Preparation Methods in X-Ray Powder Diffraction. *Powder Diffr.* **1986**, *1*, 51–63. [[CrossRef](#)]
33. Lutterotti, L. Total pattern fitting for the combined size–strain–stress–texture determination in thin film diffraction. *Nucl. Instrum. Methods Phys. Res. Sect. B Beam Interact. Mater. At.* **2010**, *268*, 334–340. [[CrossRef](#)]
34. Lutterotti, L.; Bortolotti, M.; Ischia, G.; Lonardelli, I.; Wenk, H.R. Rietveld texture analysis from diffraction images. *Z. Kristallogr. Suppl.* **2007**, *26*, 125–130. [[CrossRef](#)]
35. Lutterotti, L.; Chateigner, D.; Ferrari, S.; Ricote, J. Texture, residual stress and structural analysis of thin films using a combined X-ray analysis. *Thin Solid Film.* **2004**, *450*, 34–41. [[CrossRef](#)]
36. Tauc, J. Optical properties and electronic structure of amorphous Ge and Si. *Mater. Res. Bull.* **1968**, *3*, 37–46. [[CrossRef](#)]
37. Rueden, C.T.; Schindelin, J.; Hiner, M.C.; DeZonia, B.E.; Walter, A.E.; Arena, E.T.; Eliceiri, K.W. ImageJ2: ImageJ for the next generation of scientific image data. *BMC Bioinform.* **2017**, *18*, 529. [[CrossRef](#)]
38. Budchart, P.; Khamwut, A.; Sinthuvanich, C.; Ratanapo, S.; Poovorawan, Y.; T-Thienprasert, N.P. Partially Purified *Gloriosa superba* Peptides Inhibit Colon Cancer Cell Viability by Inducing Apoptosis Through p53 Upregulation. *Am. J. Med. Sci.* **2017**, *354*, 423–429. [[CrossRef](#)]
39. Khamwut, A.; Jevapatarakul, D.; Reamtong, O.; T-Thienprasert, N.P. In vitro evaluation of anti-epidermoid cancer activity of *Acanthus ebracteatus* protein hydrolysate and their effects on apoptosis and cellular proteins. *Oncol. Lett.* **2019**, *18*, 3128–3136. [[CrossRef](#)]
40. Leonard, M.K.; Kommagani, R.; Payal, V.; Mayo, L.D.; Shamma, H.N.; Kadakia, M.P. $\Delta Np63\alpha$ regulates keratinocyte proliferation by controlling PTEN expression and localization. *Cell Death Differ.* **2011**, *18*, 1924–1933. [[CrossRef](#)]
41. Safawo, T.; Sandeep, B.V.; Pola, S.; Tadesse, A. Synthesis and characterization of zinc oxide nanoparticles using tuber extract of anchote (*Coccinia abyssinica* (Lam.) Cong.) for antimicrobial and antioxidant activity assessment. *OpenNano* **2018**, *3*, 56–63. [[CrossRef](#)]
42. Hassan, S.S.M.; El Azab, W.I.M.; Ali, H.R.; Mansour, M.S.M. Green synthesis and characterization of ZnO nanoparticles for photocatalytic degradation of anthracene. *Adv. Nat. Sci. Nanosci. Nanotechnol.* **2015**, *6*, 045012. [[CrossRef](#)]
43. Singh, J.; Kaur, S.; Kaur, G.; Basu, S.; Rawat, M. Biogenic ZnO nanoparticles: A study of blueshift of optical band gap and photocatalytic degradation of reactive yellow 186 dye under direct sunlight. *Green Processing Synth.* **2019**, *8*, 272–280. [[CrossRef](#)]
44. Li, X.-H.; Xu, J.-Y.; Jin, M.; Shen, H.; Li, X.-M. Electrical and Optical Properties of Bulk ZnO Single Crystal Grown by Flux Bridgman Method. *Chin. Phys. Lett.* **2006**, *23*, 3356–3358. [[CrossRef](#)]
45. Debanath, M.K.; Karmakar, S. Study of blueshift of optical band gap in zinc oxide (ZnO) nanoparticles prepared by low-temperature wet chemical method. *Mater. Lett.* **2013**, *111*, 116–119. [[CrossRef](#)]
46. Huang, M.H.; Mao, S.; Feick, H.; Yan, H.; Wu, Y.; Kind, H.; Weber, E.; Russo, R.; Yang, P. Room-Temperature Ultraviolet Nanowire Nanolasers. *Science* **2001**, *292*, 1897–1899. [[CrossRef](#)]
47. Khan, M.M.; Saadah, N.H.; Khan, M.E.; Harunsani, M.H.; Tan, A.L.; Cho, M.H. Phytogenic Synthesis of Band Gap-Narrowed ZnO Nanoparticles Using the Bulb Extract of *Costus woodsonii*. *BioNanoScience* **2019**, *9*, 334–344. [[CrossRef](#)]

48. Xu, J.; Huang, Y.; Zhu, S.; Abbas, N.; Jing, X.; Zhang, L. A review of the green synthesis of ZnO nanoparticles using plant extracts and their prospects for application in antibacterial textiles. *J. Eng. Fibers Fabr.* **2021**, *16*, 15589250211046242. [[CrossRef](#)]
49. Syed Ab Rahman, S.F.; Sijam, K.; Omar, D. Chemical composition of Piper sarmentosum extracts and antibacterial activity against the plant pathogenic bacteria *Pseudomonas fuscovaginae* and *Xanthomonas oryzae* pv. *oryzae*. *J. Plant Dis. Prot.* **2014**, *121*, 237–242. [[CrossRef](#)]
50. Shi, W.; Li, C.; Li, M.; Zong, X.; Han, D.; Chen, Y. Antimicrobial peptide melittin against *Xanthomonas oryzae* pv. *oryzae*, the bacterial leaf blight pathogen in rice. *Appl. Microbiol. Biotechnol.* **2016**, *100*, 5059–5067. [[CrossRef](#)]
51. Luo, H.-Z.; Guan, Y.; Yang, R.; Qian, G.-L.; Yang, X.-H.; Wang, J.-S.; Jia, A.-Q. Growth inhibition and metabolomic analysis of *Xanthomonas oryzae* pv. *oryzae* treated with resveratrol. *BMC Microbiol.* **2020**, *20*, 117. [[CrossRef](#)] [[PubMed](#)]
52. Huang, R.-H.; Lin, W.; Zhang, P.; Liu, J.-Y.; Wang, D.; Li, Y.-Q.; Wang, X.-Q.; Zhang, C.-S.; Li, W.; Zhao, D.-L. Anti-phytopathogenic Bacterial Metabolites From the Seaweed-Derived Fungus *Aspergillus* sp. D40. *Front. Mar. Sci.* **2020**, *7*, 313. [[CrossRef](#)]
53. Kalachyova, Y.; Olshtrem, A.; Guselnikova, O.A.; Postnikov, P.S.; Elashnikov, R.; Ulbrich, P.; Rimpelova, S.; Švorčík, V.; Lyutakov, O. Synthesis, Characterization, and Antimicrobial Activity of Near-IR Photoactive Functionalized Gold Multibranched Nanoparticles. *ChemistryOpen* **2017**, *6*, 254–260. [[CrossRef](#)] [[PubMed](#)]
54. Hanley, C.; Layne, J.; Punnoose, A.; Reddy, K.M.; Coombs, I.; Coombs, A.; Feris, K.; Wingett, D. Preferential killing of cancer cells and activated human T cells using ZnO nanoparticles. *Nanotechnology* **2008**, *19*, 295103. [[CrossRef](#)]
55. Aljabali, A.A.A.; Obeid, M.A.; Bakshi, H.A.; Alshaer, W.; Ennab, R.M.; Al-Trad, B.; Al Khateeb, W.; Al-Batayneh, K.M.; Al-Kadash, A.; Alsotari, S.; et al. Synthesis, Characterization, and Assessment of Anti-Cancer Potential of ZnO Nanoparticles in an In Vitro Model of Breast Cancer. *Molecules* **2022**, *27*, 1827. [[CrossRef](#)]
56. Chelladurai, M.; Sahadevan, R.; Margavelu, G.; Vijayakumar, S.; González-Sánchez, Z.I.; Vijayan, K.; KC, D.B. Anti-skin cancer activity of *Alpinia calcarata* ZnO nanoparticles: Characterization and potential antimicrobial effects. *J. Drug Deliv. Sci. Technol.* **2021**, *61*, 102180. [[CrossRef](#)]